Journal of Power Sources 243 (2013) 195–202

Contents lists available at SciVerse ScienceDirect

Journal of Power Sources

journal homepage: www.elsevier.com/locate/jpowsour

Modeling the cathode catalyst layer of a Direct Methanol Fuel Cell

Saif Matar, Jiabin Ge, Hongtan Liu*

Clean Energy Research Institute, College of Engineering, University of Miami, Coral Gables, FL 33146, USA

HIGHLIGHTS

- A DMFC model is developed to study the effects of cathode catalyst layer thickness.
- The distribution of methanol concentration in the cathode catalyst layer is considered.
- Modeling results agree well with experimental data for difference CCL thickness.
- Neglecting methanol contamination in the CCL significantly overpredicts fuel cell performance.

ARTICLE INFO

Article history:
Received 22 February 2013
Received in revised form
21 May 2013
Accepted 23 May 2013
Available online 8 June 2013

Keywords:
DMFC
Direct methanol fuel cell
Methanol cross-over
Fuel cell
Modeling

ABSTRACT

A two-dimensional, single phase, multi-component model is developed to study the effects of cathode catalyst layer thickness on DMFC's performance. The simulations consider the effects of mixed potentials as well as the distribution of methanol concentration in the cathode catalyst layer, normally neglected by most DMFC models. In other words, the assumption of zero methanol concentration at the interface between the membrane and cathode catalyst layer (CCL) is not used in this model. COMSOL Multiphysics V4.3, a finite element analysis solver and simulation software, is employed to solve the fully coupled set of equations for electrochemical kinetics, continuity, momentum and species. There is a good agreement between the modeling results and the experimental data. Further modeling results show that neglecting methanol contamination in the CCL, i.e. assuming that methanol concentration goes to zero at the membrane/cathode interface, significantly overpredicts the fuel cell performance.

1. Introduction

Direct Methanol Fuel Cells (DMFCs) are considered a great alternative to lithium-ion batteries for powering the next generation of mobile devices. However, methanol crossover in DMFCs is a serious drawback to the cell performance and any advancement in this type of fuel cells is impeded by such a phenomenon. Two possible ways to mitigate methanol crossover and its effects are: (a) improving the electro-oxidation process in the catalyst layer, and (b) improving the structure of the catalyst and gas diffusion layers.

There are several models in the literature that focus on the effects of mixed potentials in DMFCs. Sundmacher et al. [1] developed a mathematical model that accounts for methanol crossover through the membrane. Wang and Wang [2] employed a two-phase, multicomponent model to investigate the electrochemical kinetics and transport phenomena in DMFCs including the mixed potential effects of methanol oxidation due to methanol crossover. In their model, the catalyst layers were simplified as planes with no thickness. Liu and Wang [3] studied the mixed potential in DMFCs numerically and provided detailed kinetics of methanol oxidation reaction (MOR) in the cathode. They showed the polarization curves for different cathode catalyst layer (CCL) thicknesses; however, their results do not follow the performance pattern of the experimental ones shown in Ref. [4]. Yin [5] proposed an algebraic model that studies the simultaneous effects of water and methanol crossover. The model treated the catalyst layers as infinitely thin interfaces and assumed that the crossed-over methanol is consumed instantaneously at the membrane/electrode interface. Recently, Kulikovsky [6] considered a direct catalytic reaction between methanol and oxygen in the CCL and compared the result with the assumption of an electrochemical reaction of methanol in the cathode [7].

In a previous experimental work [4], the effects of CCL thickness on the detrimental effect of methanol crossover in a DMFC under various operating conditions were studied. The results showed that when a thicker CCL was used, the fuel cell performance increased significantly. This was attributed to the oxidation of the crossed-over methanol in part of the catalyst layer and leaving the rest of

* Corresponding author. Tel.: +1 305 284 2019; fax: +1 305 284 2580.
E-mail address: hliu@miami.edu (H. Liu).

0378-7753/$ – see front matter © 2013 Elsevier B.V. All rights reserved.
http://dx.doi.org/10.1016/j.jpowsour.2013.05.122

Nomenclature

a	specific surface area
ACH	anode channel
ACL	anode catalyst layer
AGDL	anode gas diffusion layer
CCL	cathode catalyst layer
C	methanol concentration
CL	catalyst layer
CO_2	carbon dioxide
D	diffusion coefficient
E	voltage
E^o	equilibrium potential
e^-	electron
ECA	electrochemically active area
EOD	electro osmotic drag
F	Faraday constant
GDL	gas diffusion layer
H^+	proton
H_2	hydrogen
H_2O	water
I	current
i_o^{ref}	reference exchange current density
j	current per unit volume
M	molecular weight
m_{pt}	catalyst loading
MeOH	methanol
MOR	methanol oxidation reaction
N	flux
N_2	nitrogen
O_2	oxygen
ORR	oxygen reduction reaction
P, p	pressure, partial pressure
PEM	proton exchange membrane
R	resistance or gas constant
S	source term
T	temperature
$\mathbf{u}$	velocity
w	mass fraction
x	mole fraction

Greek letters

α	transfer coefficient
γ	reaction order
δ	thickness
ε	porosity
η	activation overpotential
κ	permeability
μ	dynamic viscosity
ρ	density
σ	conductivity
ϕ	potential
ω	a function of methanol concentration

Subscripts

a	anode
c	cathode
ct	charge transfer
m	membrane
mixed	mixed potential
s	solid phase
xover	methanol crossover

Superscripts

eff	effective
M	membrane
ref	reference

the catalyst layer free from methanol contamination, thus leading to mitigations of the effects of mixed potentials. In this paper, a single-phase model was developed to model methanol crossover in DMFCs. The model was used to study the effect of changing the thickness of the CCL on the cell performance. To focus on the effect of the CCL thickness, as shown in the previous experimental results, the effect of liquid water in the CCL was not explicitly studied. The model basically assumesd the effects of liquid water in blocking the active reaction sites for all the three cases with different CCL thicknesses were the same. The simulations considered the effects of mixed potential as well as the distribution of methanol concentration in the CCL that is normally neglected in most of DMFC models. In this modeling, methanol oxidation occurs in the entire CCL unless the local methanol concentration reaches zero.

2. Model description and assumptions

Fig. 1 shows a schematic drawing of a DMFC in the XY plane. The modeling domain consists of the anode and cathode flow channels, gas diffusion layers (GDLs), catalyst layers (CLs), and the Nafion® membrane. In the anode side, the aqueous methanol flows in the channel and then diffuses through the porous GDL until it reaches the catalyst layer, where it is electrochemically oxidized according to the reaction given in Eq. (1). The protons, water and the crossed-over methanol transfer through the membrane. On the cathode side, air flows in the channel and then it is transported to the reaction sites via diffusion and convection, where oxygen reacts with the protons coming from the anode through the membrane and the

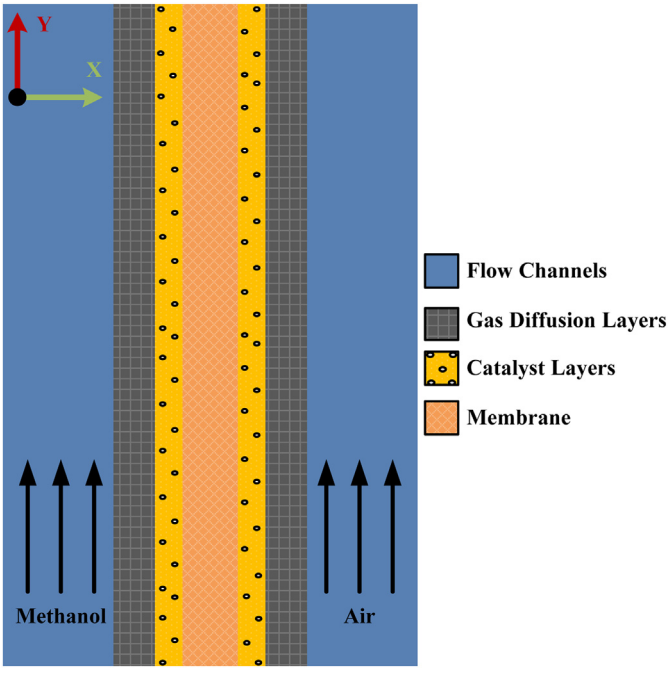

Fig. 1. Schematic of the modeling domain.

electrons coming from the external circuit to form water as described by Eq. (2).

$$\text{Anode}: CH_3OH + H_2O \rightarrow 6H^+ + 6e^- + CO_2 \quad (1)$$

$$\text{Cathode}: \frac{3}{2}O_2 + 6H^+ + 6e^- \rightarrow 3H_2O \quad (2)$$

$$\text{Overall}: CH_3OH + \frac{3}{2}O_2 \rightarrow 2H_2O + CO_2 \quad (3)$$

The following assumptions were made in the development of the model: (1) flow is laminar, fully developed and incompressible, (2) the mixture of reactant gasses is considered to be ideal, (3) the cell is assumed to operate under steady state conditions, (4) the process is isothermal, (5) the effects of CO_2 are negligible; i.e. single phase assumption, and (6) the membrane is fully hydrated.

3. Governing equations

3.1. Electrochemical kinetics

The electro-oxidation of methanol at the anode and the electro-reduction of oxygen at the cathode are described by Tafel kinetics to determine the anodic (j_a) and cathodic (j_c) transfer current densities:

$$j_a = ai_{o,a}^{ref}\left(\frac{C_{MeOH}}{C_{MeOH}^{ref}}\right)^{\gamma_a}\exp\left(\eta_a\frac{\alpha_a F}{RT}\right) \quad (4)$$

$$j_c = ai_{o,c}^{ref}(1-\omega)\left(\frac{C_{O_2}}{C_{O_2}^{ref}}\right)^{\gamma_c}\exp\left(\eta_c\frac{\alpha_c F}{RT}\right) \quad (5)$$

where ai_a^{ref} and ai_c^{ref} are the reference exchange currents densities multiplied by the specific surface area (a) at the anode and cathode sides, respectively, γ_a and γ_c are the anode and cathode reaction orders, η_a and η_c are the anode and cathode activation over-potentials and α_a and α_c are the anode and cathode transfer co-efficients, respectively. C_{MeOH} and C_{O_2} are methanol and oxygen concentrations in the catalyst layers; the superscript (ref) means reference concentrations. $(1-\omega)$ accounts for the fraction of the electrochemical active area (ECA) that is available for the Oxygen Reduction Reaction (ORR):

$$\omega = \begin{cases} 0 \mid \text{All of the ECA is available for ORR} \\ 1 \mid \text{None of the ECA is availabe for ORR} \end{cases} \quad (6)$$

where ω is a function of methanol concentration in the CCL (C_{MeOH}^{CCL}) and it is defined by:

$$\omega = \frac{C_{MeOH}^{CCL}}{C_{MeOH}^{M|CCL}} \quad (7)$$

where $C_{MeOH}^{M|CCL}$ is the methanol concentration at the interface between the CCL and the membrane.

The specific surface area (a) is defined by Marr and Li [8]:

$$a = \frac{m_{pt}ECA}{\delta^{CL}} \quad (8)$$

where m_{pt} is the catalyst loading and δ^{CL} is the catalyst layer thickness. The reference exchange current densities for the MOR and the ORR are given by Wang and Wang [2] and Parthasarathy et al. [9]:

$$i_{o,a}^{ref} = 94.25\exp\left[\frac{35570}{R}\left(\frac{1}{353}-\frac{1}{T}\right)\right] \quad (9)$$

$$i_{o,c}^{ref} = 0.0422\exp\left[\frac{73200}{R}\left(\frac{1}{353}-\frac{1}{T}\right)\right] \quad (10)$$

The activation overpotential (η_k) is related to the solid phase (φ_s) and membrane phase (φ_m) potentials as follows:

$$\eta_k = \Phi_k - E_k^o \quad (11)$$

in which,

$$\Phi_k = \varphi_{s,k} - \varphi_m \quad (12)$$

where the subscript k denotes either a for anode or c for cathode and E_k^o is the equilibrium potential of the electrode. The cell voltage (E_{cell}) is calculated by:

$$E_{cell} = \Phi_c - \Phi_a \quad (13)$$

Rearranging Eq. (11) and substituting into Eq. (13) yields:

$$E_{cell} = \Delta E^o - \eta_a + \eta_c \quad (14)$$

If ohmic losses are considered, then the cell voltage for kinetic controlled conditions (no mass transport limitations) is:

$$E_{cell} = \Delta E^o - \eta_a + \eta_c - I_{cell}R_m \quad (15)$$

where ΔE^o is the thermodynamic equilibrium potential of the cell, R_m is the area specific resistance of the membrane and it is related to the thickness (δ^M) and the ionic conductivity of the membrane (σ_m) by:

$$R_m = \frac{\delta^M}{\sigma_m} \quad (16)$$

and for a fully hydrated membrane, σ_m is calculated from the correlation provided by Springer el al. [10]:

$$\sigma_m(T) = 11.0986\times10^{-2}\exp\left[1268\left(\frac{1}{303}-\frac{1}{T}\right)\right] \quad (17)$$

The cell current density (I_{cell}) can be found by:

$$I_{cell} = \frac{1}{L}\iint_{ACL} j_a dxdy \quad (18)$$

When solving the equations, the following balance must be satisfied,

$$I_{cell} + I_{xover} = \frac{1}{L}\iint_{CCL} j_c dxdy \quad (19)$$

where I_{xover} is the equivalent methanol crossover current density and L is the length of the cell.

Vielstich et al. [11] reported that a pure chemical reaction path for methanol oxidation in the cathode is possible. They also reported that the rate of formation of CO_2 was measured as 4.2×10^{-7} mol s^{-1} at 0.3 V. In general, the volumetric reaction rate (r) can be defines as:

$$r = \theta r_c(C_{MeOH})^{\beta}(C_{O_2})^{\gamma} \quad (20)$$

where r_c is the rate constant of the reaction, β and γ are stoichiometric exponents and θ is an empirical coefficient. According to the DMFC overall reaction, Eq. (3), one can deduce that:

$$\begin{aligned} r_{MeOH} &= r \\ r_{O_2} &= 1.5r \\ r_{CO_2} &= r \\ r_{H_2O} &= 2r \end{aligned} \tag{21}$$

3.2. Flow and species governing equations

Continuity: The conservation of mass is expressed as

$$\rho \nabla \cdot \mathbf{u} = 0 \tag{22}$$

where $\mathbf{u}$ is the velocity and ρ is the density.

Momentum: Navier–Stokes equation, Eq. (23), is used to describe the flow in the flow channels and Brinkman equation, Eq. (24), for the flow in the porous mediums [12]:

$$\rho(\mathbf{u}\cdot\nabla)\mathbf{u} = \nabla\cdot\left[-PI + \mu\left(\nabla\mathbf{u} + (\nabla\mathbf{u})^{T}\right)\right] \tag{23}$$

$$\frac{\rho}{\varepsilon^{\ell}}\left((\mathbf{u}\cdot\nabla)\frac{\mathbf{u}}{\varepsilon^{\ell}}\right) = \nabla\cdot\left[-PI + \frac{1}{\varepsilon^{\ell}}\left\{\mu\left(\nabla\mathbf{u} + (\nabla\mathbf{u})^{T}\right) - \frac{2}{3}\mu(\nabla\cdot\mathbf{u})I\right\}\right] - \frac{\mu}{\kappa^{\ell}}\mathbf{u} \tag{24}$$

where μ is the dynamic viscosity, P is the pressure, I is the identity matrix, ε and κ are the porosity and the permeability of the porous medium and the superscript ℓ denotes either the gas diffusion layer (GDL) or the catalyst layer (CL). Note that $\mathbf{u} = 0$ in the membrane.

Species: The transport of species in the anode and in the cathode is governed by a combination of diffusion and convection:

$$\rho(\mathbf{u}\cdot\nabla)w_i = \rho D_i^{eff}\nabla^2 w_i + S_i \tag{25}$$

where w_i is the mass fraction of species i, and D_i^{eff} is the effective diffusivity. The source term S_i accounts for the consumption or production (electrochemically and chemically) of species i and it is only applicable in the catalyst layer; Table 1 shows the source term for different species. Note that,

$$\sum_i x_i = 1, \quad \sum_i w_i = 1, \quad \sum_i S_i = 0 \tag{26}$$

The mass fraction can be calculated from the molar fraction (x_i) by:

$$w_i = x_i\frac{M_i}{\overline{M}} \tag{27}$$

where M_i is the molecular weight of species i and $\overline{M}$ is the average molecular weight of the mixture. The local mole fraction of methanol (x_{MeOH}) is defined by:

$$x_{MeOH} = \frac{C_{MeOH}}{C_{MeOH} + C_{H_2O}} \tag{28}$$

Table 1
S_i for different species.

	Species	S_i
Anode	MeOH	$-\frac{M_{MeOH}}{6F}j_a$
	H_2O	$-\frac{M_{H_2O}}{6F}j_a$
Cathode	O_2	$\left(-\frac{1}{4F}j_c - 1.5r\right)M_{O_2}$
	H_2O	$\left(\frac{1}{2F}j_c + 2r\right)M_{H_2O}$
	$MeOH_{xover}$	$-rM_{MeOH}$

Table 2
Diffusion volumes.

Species	Diffusion volume ($m^3\ mol^{-1}$)
O_2	16.6×10^{-6}
N_2	17.9×10^{-6}
H_2O	12.7×10^{-6}

Since methanol concentration is negligible compared to that of water, then:

$$x_{MeOH} \cong \frac{C_{MeOH}}{C_{H_2O}} = C_{MeOH}\frac{M_{H_2O}}{\rho_{H_2O}} \tag{29}$$

Moreover, the physical properties of the solution will retain those of water and can be determined by [13,14]:

$$\rho = 1000 - 0.0178(T - 277.15)^{1.7} \tag{30}$$

$$\mu = 0.458509 - 5.30474 \times 10^{-3}T + 2.31231 \times 10^{-5}T^2 - 4.49161 \times 10^{-8}T^3 + 3.27681 \times 10^{-11}T^4 \tag{31}$$

The effective diffusion coefficient of methanol (D_{MeOH}^{eff}) in water is given by Yaws [15]:

$$D_{MeOH}^{eff} = \begin{cases} D_{MeOH}^{ACH} = 10^{-5.4163 - \frac{999.787}{T}} \\ D_{MeOH}^{AGDL} = \varepsilon_{AGDL}^{1.5} D_{MeOH}^{ACH} \\ D_{MeOH}^{ACL} = \varepsilon_{ACL}^{1.5} D_{MeOH}^{ACH} \end{cases} \tag{32}$$

where, D_{MeOH}^{ACH}, D_{MeOH}^{AGDL} and D_{MeOH}^{ACL} are methanol diffusivities in the anode channel, anode gas diffusion layer and anode catalyst layer, respectively. The Bruggeman correction is used in Eq. (32) in order to take into account the resistance to diffusion in the porous medium.

The transfer of methanol through the Nafion® membrane occurs via diffusion and electro-osmosis. The transport due to convection can be ignored owing to the negligible pressure difference across the membrane [16]. Therefore,

$$N_{MeOH}^{M} = -D_{MeOH}^{M}\nabla C_{MeOH}^{M} + n_{MeOH}^{EOD}\frac{I_{cell}}{F} \tag{33}$$

where N_{MeOH}^{M} is the flux of methanol through the membrane, n_{MeOH}^{EOD} is methanol electro-osmatic drag coefficient and D_{MeOH}^{M} is the diffusion coefficient of methanol in Nafion® and it is given by Kulikovsky [17]:

$$D_{MeOH}^{M} = 4.012 \times 10^{-9}\exp(0.024312T) \tag{34}$$

The methanol crossover equivalent current density (I_{xover}) is determined by:

$$I_{xover} = 6FN_{MeOH}^{M} \tag{35}$$

Table 3
Geometric parameters.

Parameter	Value
Cell length	30 mm
Channel width	2 mm
Channel depth	1 mm
Land width	1 mm
GDL thickness	0.381 mm
Membrane thickness	0.1778 mm

Table 4
Physiochemical parameters.

Parameter	Value
Operating conditions	
Cell temperature (T)	343.15 K
Pressure (P)	1 atm
Inlet conditions	
Methanol inlet concentration	1000 mol m^{-3}
Methanol reference concentration	2000 mol m^{-3}
Methanol inlet flow rate	6 ml min^{-1}
Oxygen inlet mass fraction	0.183
Oxygen reference concentration	3.39 mol m^{-3}
Oxygen inlet flow rate	600 sccm
Porosity, permeability, conductivity	
GDL	0.8
	1.18×10^{-11} m^2
	222 S m^{-1}
CL	0.4
	2.36×10^{-12} m^2
	222 S m^{-1}
Electrochemical parameters	
Anodic specific surface area (a)	8×10^4 m^{-1}
Anodic transfer coefficient (α_a)	0.28
Anode reaction order (γ_a)	1
Cathode reaction order (γ_c)	1

According to Ren et al. [18], methanol electro-osmatic drag is defined by:

$$n_{MeOH}^{EOD} = n_{H_2O}^{EOD} x_{MeOH} \tag{36}$$

where $n_{H_2O}^{EOD}$ is the electro-osmatic drag of water through the Nafion® membrane and x_{MeOH} is the molar fraction of methanol at the interface between anode catalyst layer and the membrane. Guo and Ma [19] provided a fitted correlation for $n_{H_2O}^{EOD}$ in terms of temperature:

$$n_{H_2O}^{EOD} = 2.9\exp\left[1029\left(\frac{1}{333} - \frac{1}{T}\right)\right] \tag{37}$$

The transport of water through the Nafion® membrane is due to electro-osmatic drag only. The diffusive transport is neglected with the assumption that both the anode and cathode are fully hydrated. Therefore, the flux of water through the membrane ($N_{H_2O}^{M}$) can be found from:

$$N_{H_2O}^{M} = n_{H_2O}^{EOD} \frac{I_{cell}}{F} \tag{38}$$

For fully humidified air, the partial pressure (P_{H_2O}) (bar) of saturated water vapor is determined by [10]:

$$p_{H_2O} = 10^{-2.1794+0.02953T-9.1837\times10^{-5}T^2+1.4454\times10^{-7}T^3} \tag{39}$$

Then the mole fraction of water vapor ($x_{H_2O,c}$) in the air stream (assuming an ideal gas mixture) is:

$$x_{H_2O,c} = \frac{p_{H_2O}}{p_{air}} \tag{40}$$

and, therefore, oxygen (x_{O_2}) and nitrogen (x_{N_2}) mole fractions can be defined as:

$$x_{O_2} = 0.21(1 - x_{H_2O,c}) \tag{41}$$

$$x_{N_2} = 0.79(1 - x_{H_2O,c}) \tag{42}$$

The multicomponent Fick diffusivities for the species in the cathode are related to multicomponent Maxwell–Stefan diffusivities, D_{ik}, by [12]:

$$\frac{x_i x_k}{D_{ik}} = -m_i m_k \left(\sum_{j \neq i} (\mathrm{adjB}_i)_{jk} / \sum_{j \neq i} \tilde{D}_{ij} (\mathrm{adj}B_i)_{jk} \right) \tag{43}$$

in which,

$$(B_i)_{kj} = \tilde{D}_{kj} - \tilde{D}_{ij}, i \neq j \tag{44}$$

where $(\mathrm{adjB}_i)_{jk}$ is the jk^{th} component of the adjoint of the matrix B_i. An empirical equation based on the kinetic gas theory can be used to calculate D_{ik} [20]:

$$D_{ik} = \theta \frac{T^{1.75}}{P\left(v_i^{1/3} + v_k^{1/3}\right)^2} \left(\frac{1}{M_i} - \frac{1}{M_k}\right)^{1/2} \tag{45}$$

where θ is a constant $= 3.16 \times 10^{-8}$ Pa m^2 s^{-1}, T is the temperature, P is the pressure and v_i is the molar diffusion volume of species i. The molar diffusion volumes for O_2, N_2 and H_2O are listed in Table 2 [21].

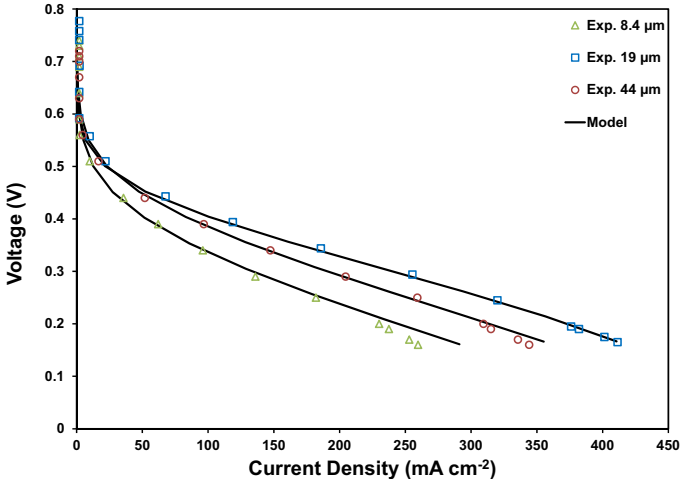

Fig. 2. Comparison of the modeling results with the experimental data for different cathode catalyst layer thicknesses.

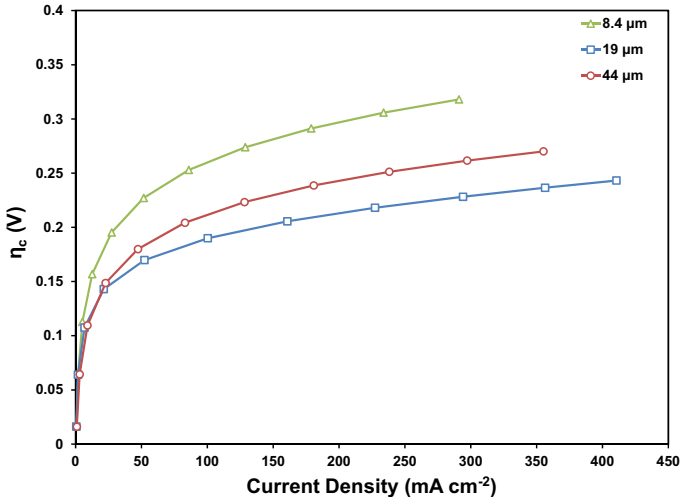

Fig. 3. Cathode overpotential performance curves for different cathode catalyst layer thicknesses.

4. Solution strategy

COMSOL Multiphysics V4.3, a finite element analysis solver and simulation software, is employed to solve the governing equations. The mass fractions of methanol (w_{MeOH}) and water ($w_{H_2O,a}$) in the anode, and oxygen (w_{O_2}), nitrogen (w_{N_2}), and water ($w_{H_2O,c}$) in the cathode are solved for in the flow channels, GDLs and catalyst layers. The boundary conditions are: inlet mass fractions or inlet concentrations and zero flux conditions at other external boundaries.

The velocity (**u**) and the pressure (P) are solved by the Navier–Stokes equation in the flow channels and by the Brinkman equation in the GDLs and the catalyst layers. The boundary conditions are: laminar inlet flow velocity and zero pressure at the outlet. Moreover, no-slip conditions are applied to the other walls.

Ohms law is used to solve for the electronic potential (φ_s) in the GDLs and the CLs and the ionic potential (φ_m) in the CLs and the membrane. The local current densities rely on φ_s and φ_m in the CLs as well as local reactant concentrations. The boundary conditions are: $\varphi_s = 0$ at the anode land, and φ_s at the cathode land is set to the cell voltage; the rest of the external boundaries are electrically insulated.

The equations are fully coupled; the species, Navier–Stokes and Brinkman equations are coupled to the electrochemical kinetics via the source terms. Couplings between the species equation and the equations of Navier–Stokes and Brinkman are made via the velocity field, pressure and the local density.

5. Results and discussions

5.1. Comparison with experimental results

The geometric parameters used in this modeling work are based on the experimental study done in Ref. [4] and are listed in Table 3. The physiochemical properties and operating conditions used in the simulations are given in Table 4. The modeled polarization curves of the MEAs with different CCL thicknesses at 1 M methanol concentration and a flow rate of 6 ml min^{-1} are compared against the experimental results in Fig. 2. It can be seen that there is a good agreement between the modeling results and the experimental data.

5.2. Effect of methanol contamination in the CCL

Methanol crossover causes an extra loss to the cell voltage, as given in Eq. (15), due to the mixed potential term in the cathode overpotential shown in Eq. (46):

$$\eta_c = \eta_{ORR} + \eta_{mixed} \quad (46)$$

where η_{ORR} is the ORR activation overpotential in the absence of methanol contamination/crossover and η_{mixed} is the mixed potential due to methanol crossover. One can deduce that any increase in the DMFC cell voltage due to improved electro-oxidation process in the cathode catalyst layer is mainly the result of a lower η_{mixed} value, but the effects of η_{ORR} cannot be ignored.

Therefore, the cathode overpotential performance curves for different CCL thicknesses were plotted and the results are shown in Fig. 3. It can be seen that the MEA with the base thickness of 8.4 μm has the highest cathode overpotential which indicates a much higher η_{mixed} and η_{ORR}. When the cathode catalyst layer thickness was increased from the 8.4 μm to 19 μm, much lower cathode overpotential was achieved. A further increase in CCL thickness from 19 μm to 44 μm resulted in an increase in the cathode overpotential, but it is still better than the base case. However, by carefully inspecting Fig. 3, it is obvious that both 19 μm and 44 μm thicknesses have the same cathode overpotential in the low current density region. This suggests that both thicknesses were capable of reducing the effects of η_{mixed}. So why is there a difference in the cathode overpotential at high current densities? It is believed that as the current increases, the η_{ORR} for the case of 44 μm CCL is

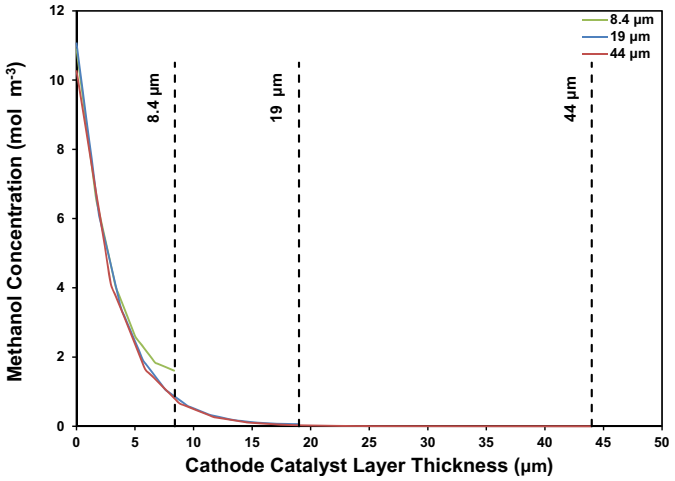

Fig. 4. Methanol concentration profiles for different cathode catalyst layer thicknesses at 0.45 V.

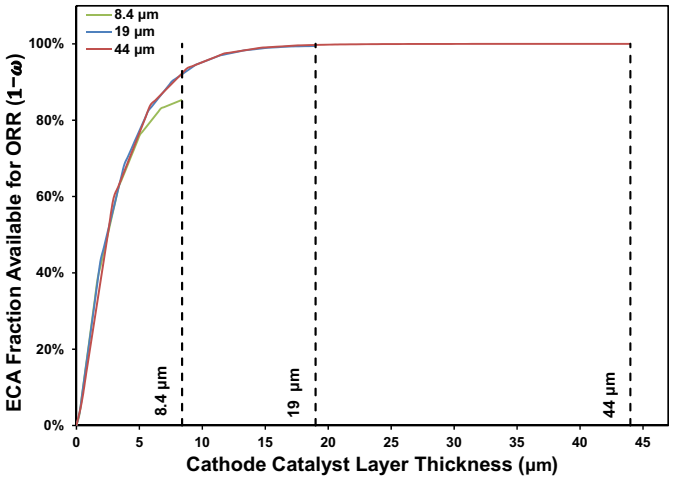

Fig. 5. Fraction of ECA $(1-\omega)$ available for the ORR at 0.45 V.

greater than the case of 19 μm CCL. Therefore, 19 μm CCL thickness gives the lowest cathode overpotential due to both low η_{ORR} and low η_{mixed}.

Another way to visualize methanol contamination in the CCL is by looking at methanol concentration profile and the fraction of ECA available for the ORR for each of the CCL thicknesses; presented in Figs. 4 and 5, respectively. Each curve in Fig. 5 can be fitted using a polynomial function and then the equation is integrated from 0 to the corresponding CCL thickness to get the ECA available for ORR. Table 5 shows the pristine ECA [4], the contaminated ECA and the ECA available for ORR, all in (cm^2_{Pt} mg^{-1}_{Pt}).

The concentration profiles in Fig. 4 are similar to the hypothesized ones in Ref. [4]. Again, for the base case, when the CL is too thin, the entire CL is flooded with methanol which resulted in a smaller area available for oxygen reduction. It can be seen from Table 5 that 61% of the ECA is available for the ORR. As the CCL thickness increases from 8.4 μm to 19 μm, part of the CL can be free from methanol contamination. Thus the active catalyst area available for oxygen reduction is greater. The modeling results show that only 18% of the ECA is contaminated with methanol in the case of 19 μm CCL thickness; about 3 μm of the 19 μm is free from methanol contamination. Although 92% of the ECA is available for the ORR when the thickness of the catalyst layer is further increased to 44 μm, the performance is lower. This, as explained in Ref. [4], mainly due to the higher mass transfer loss for oxygen transfer and the higher ohmic loss due to the additional transfer paths for oxygen, ions and electrons through the thicker CCL.

Now, the modeling results can be combined with those obtained experimentally in Ref. [4]; Table 6 is a summary of the findings. CCL with 8.4 μm thickness performed the worst due to high charge transfer resistance (R_{ct}), high ORR activation overpotential and high mixed potential. These parameters were significantly improved when the CCL thickness was increased to 19 μm which resulted in the best performance. The mixed potential is still low when the thickness was increased further to 44 μm; however, a slightly higher charge transfer resistance and η_{ORR} made the performance of 44 μm to fall between the performances of the other two thicknesses.

Table 5
ECA values for different CCL thicknesses.

CCL thickness (μm)	Pristine ECA [4]	ECA available for ORR	Contaminated ECA
8.4	282.88	172.56	110.32
19	254.37	208.58	45.79
44	243.28	223.82	19.46

Table 6
Combined modeling and experimental results.

CCL thickness (μm)	R_{ct}	η_{ORR}	η_{mixed}	Performance
8.4	− −	− −	− −	Worst
19	+ +	+ +	+ +	Best
44	− +	− +	+ +	Middle

5.3. Effect of neglecting methanol contamination in the cathode

In this simulation of the CCL, methanol oxidation occurs in the entire CCL unless the local methanol concentration reaches zero. The majority of DMFC models reported in the literature assume that methanol concentration at the interface between the membrane and CCL is zero. In other words, the effects of methanol contamination in the CCL are neglected.

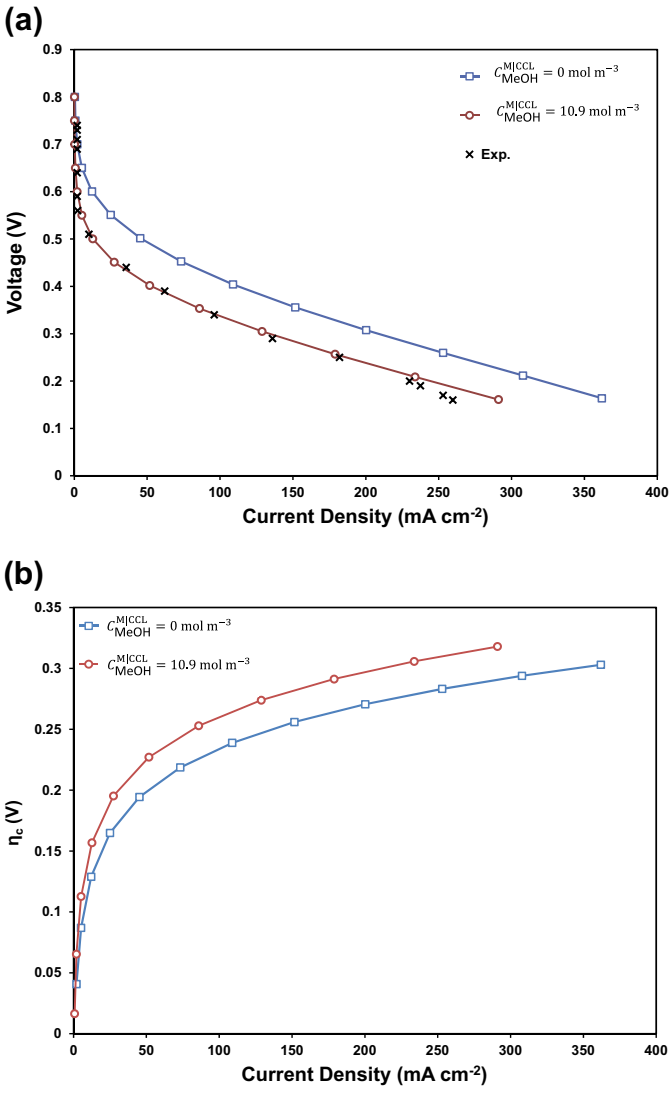

Fig. 6. The effect of assuming 0 methanol concentration at the membrane/cathode interface for 8.4 μm CCL thickness; (a) cell performance (b) cathode overpotential curves.

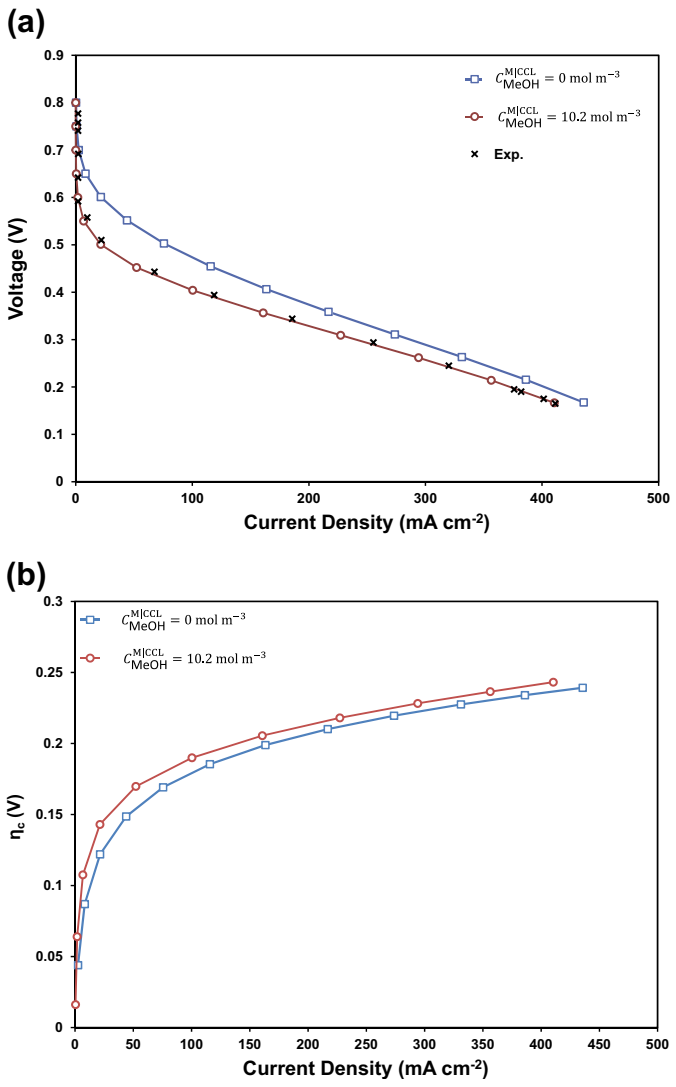

Fig. 7. The effect of assuming 0 methanol concentration at the membrane/cathode interface for 19 μm CCL thickness; (a) cell performance (b) cathode overpotential curves.

The perception that methanol concentration goes to zero at the membrane/cathode interface is probably an over simplification. The reason for this is that when methanol permeates to the cathode side, it is oxidized to produce CO_2 and water, this in turn, reduces oxygen concentration that is available for the ORR. Figs. 6 and 7 show the effects of assuming 0 methanol concentration at the interface for 8.4 μm and 19 μm CCL thicknesses. It can be seen that the performance for the case of 0 concentration is much higher than the case with methanol contamination. Therefore, it is recommended to consider the true concentration of methanol in the CCL.

6. Conclusions

In this work, a two-dimensional, single-phase, multi-component model was developed to study methanol crossover in DMFCs. The model was used to study the effect of changing the thickness of CCL on the cell performance. The simulations considered the effects of mixed potential as well as the distribution of methanol concentration in the CCL that is normally neglected in most DMFC models. In this modeling work, the methanol concentration in the entire CCL was taken into consideration, thus, the effects of both the methanol contamination of the cathode ECA and the reduction of oxygen concentration in the CCL due to methanol oxidation were included.

COMSOL Multiphysics V4.3, a finite element analysis solver and simulation software, was employed to solve the fully coupled set of equations for electrochemical kinetics, continuity, momentum and species. The modeling results of the polarizations curves for the three cases with different cathode catalyst layer thicknesses agreed very well with the experimental data. The following conclusions can be made from the combined modeling and the experimental results:

- With a thin CCL (e.g. 8.4 μm), the entire CCL could be flooded by the crossed-over methanol, causing severe contamination and resulting in high charge transfer resistance, high ORR activation overpotential, high mixed potential, and thus lower performance.
- With a relatively thicker CCL (e.g. 19 μm), the crossed-over methanol could be effectively oxidized in part of the CCL and leave the remaining portion free from contamination, leading to significantly improved performance.
- With a very thick CCL (e.g. 44 μm), though the mixed potential is low, a slightly higher charge transfer resistance and η_{ORR} caused the cell performance to decrease compared with the case with a 19 μm CCL, but still better than the case with 8.4 μm CCL.
- The modeling results showed that the assumption of zero methanol concentration at the membrane/cathode interface significantly overpredicts DMFC performance.

References

[1] K. Sundmacher, T. Schultz, S. Zhou, K. Scott, M. Ginkel, E.D. Gilles, Chemical Engineering Science 56 (2) (2001) 333–341.
[2] Z.H. Wang, C.Y. Wang, Journal of The Electrochemical Society 150 (2003) A508.
[3] F. Liu, C.Y. Wang, Journal of The Electrochemical Society 154 (2007) B514–B522.
[4] Saif Matar, Hongtan Liu, Electrochimica Acta 56 (1) (2010) 600–606.
[5] K.M. Yin, Journal of Power Sources 179 (2) (2008) 700–710.
[6] A.A. Kulikovsky, Electrochimica Acta 62 (2012) 185–191.
[7] A.A. Kulikovsky, Electrochimica Acta 79 (2012) 52–56.
[8] C. Marr, X. Li, Journal of Power Sources 77 (1) (1999) 17–27.
[9] A. Parthasarathy, S. Srinivasan, A.J. Appleby, C.R. Martin, Journal of The Electrochemical Society 139 (1992) 2530–2537.
[10] T.E. Springer, T.A. Zawodzinski, S. Gottesfeld, Journal of The Electrochemical Society 138 (1991) 2334.
[11] W. Vielstich, V.A. Paganin, F.H.B. Lima, E.A. Ticianelli, Journal of The Electrochemical Society 148 (2001) A502.
[12] COMSOL User's Guide Version 4.2, COMSOL AB, Stockholm, Sweden, 2011.
[13] F.M. White, Fluid Mechanics, fifth ed., McGraw-Hill, New York, 2003.
[14] F.D. Incropera, D.P. DeWitt, Fundamentals of Heat and Mass Transfer, John Wiley & Sons, New York, 1995.
[15] C.L. Yaws, Handbook of Transport Property Data: Viscosity, Thermal Conductivity and Diffusion Coefficients of Liquids and Gases, Gulf Publishing Company, Houston, TX, 1995.
[16] J. Han, H. Liu, Journal of Power Sources 164 (1) (2007) 166–173.
[17] A.A. Kulikovsky, Journal of Applied Electrochemistry 30 (2000) 1005–1014.
[18] X. Ren, T.E. Springer, T.A. Zawodzinski, S. Gottesfeld, Journal of The Electrochemical Society 147 (2) (2000) 466–474.
[19] H. Guo, C.F. Ma, Electrochemistry Communications 6 (3) (2004) 306–312.
[20] J.A. Wesselingh, R. Krishna, Mass Transfer in Multicomponent Mixtures, Delft University Press, 2000.
[21] R. Perry, D. Green, Perry's Chemical Engineering Handbook, seventh ed., McGraw-Hill, 1997.